Supplemental Data for

MYC-dependent oxidative metabolism regulates osteoclastogenesis via nuclear receptor ERRα

Seyeon Bae, Min Joon Lee, Se Hwan Mun, Eugenia G. Giannopoulou, Vladimir Yong-Gonzalez, Justin R. Cross, Koichi Murata, Vincent Giguère, Marjolein van der Meulen, and Kyung-Hyun Park-Min

This PDF file includes:

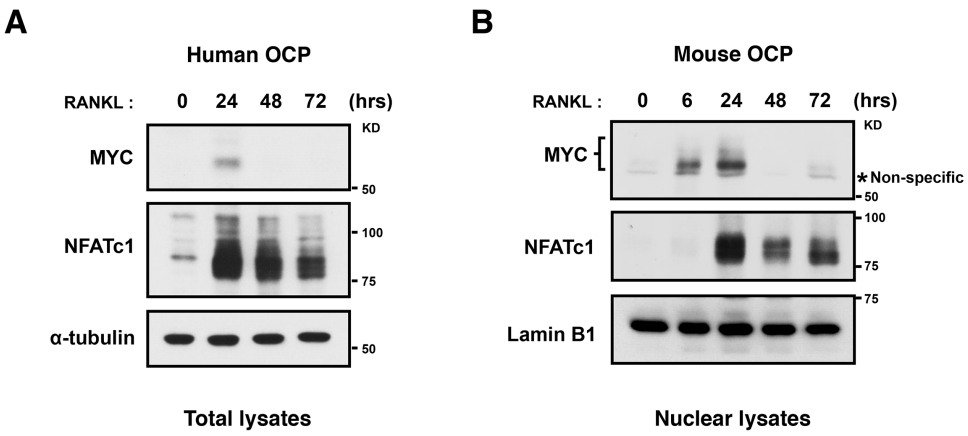

Supplemental Figure 1. Expression of MYC in osteoclast differentiation.

Either (**A**) human OCPs or (**B**) mouse OCPs were cultured with RANKL (50 ng/ml) for the indicated time points and immunoblot of (**A**) whole-cell lysates or (**B**) nuclear lysates was measured using MYC, NFATc1, and α-tubulin or lamin B antibodies. α-tubulin and lamin B served as a loading control for total and nuclear lysates, respectively. Representative results from 3 experiments are shown.

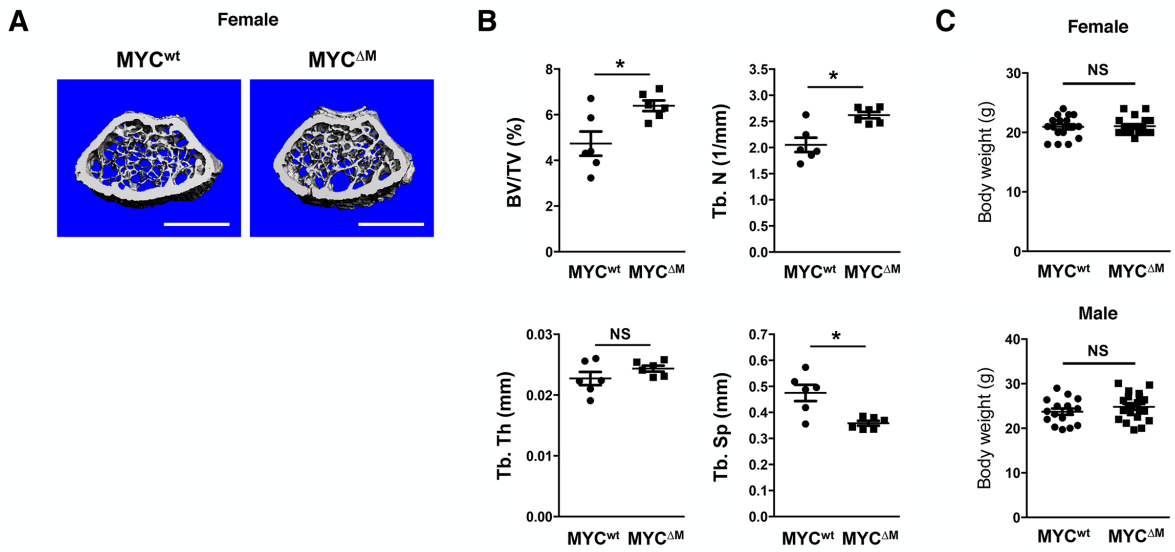

Supplemental Figure 2. Myeloid-specific MYC-deficient female mice exhibit high bone mass.

Microcomputed tomography (μCT) analysis of the femurs of 12-week-old female myeloid-specific MYC deficient mice ($MYC^{\Delta M}$) and their littermate MYC^{wt} (n=6). (**A**) Representative images showing trabecular architecture by μCT reconstruction in the distal femurs. Scale bars, 1 mm. (**B**) μCT measurements for the indicated parameters in the distal femurs. Bone volume (BV/TV), trabecular number (Tb.N.), trabecular thickness (Tb.Th.), and trabecular space (Tb.Sp.) were determined by μCT analysis. (**C**) The body weight of 12-week-old female and male $MYC^{\Delta M}$ mice and their respective control MYC^{wt} mice ($n \geq 16$). Data are shown as mean ± SEM. *P < 0.05; NS, not significant by two-tailed, unpaired t-test.

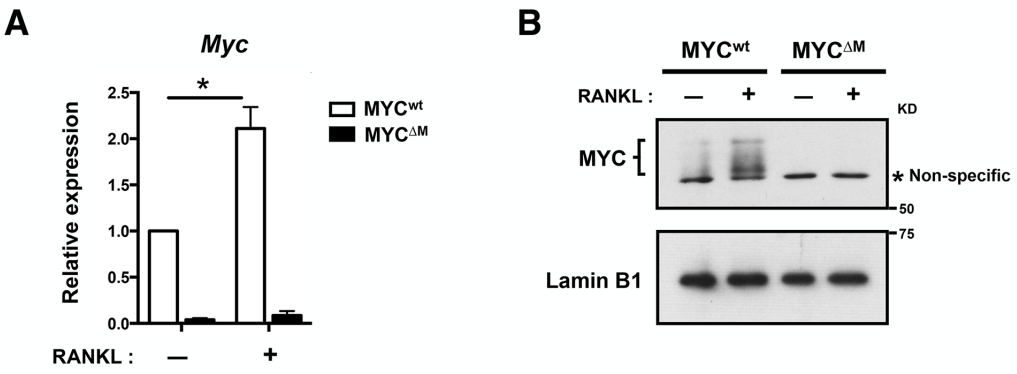

Supplemental Figure 3. The mRNA and protein expression of MYC in control and MYC-deficient OCPs after RANKL stimulation.

Control (MYC^{wt}) and MYC-deficient ($MYC^{\Delta M}$) OCPs were stimulated with RANKL (50 ng/ml) for the indicated times. (**A**) The mRNA expression of *Myc* (relative to the *Hprt* housekeeping gene) in control and MYC-deficient OCPs after RANKL stimulation for 24 hrs (n=8). Data are shown as mean ± SEM. *$P < 0.05$ by Two-way ANOVA with a *post hoc* Tukey test. (**B**) The protein expression of MYC was determined by immunoblot using nuclear lysates after RANKL stimulation for 8 hrs. Lamin B served as a loading control. Data are representative of 4 experiments.

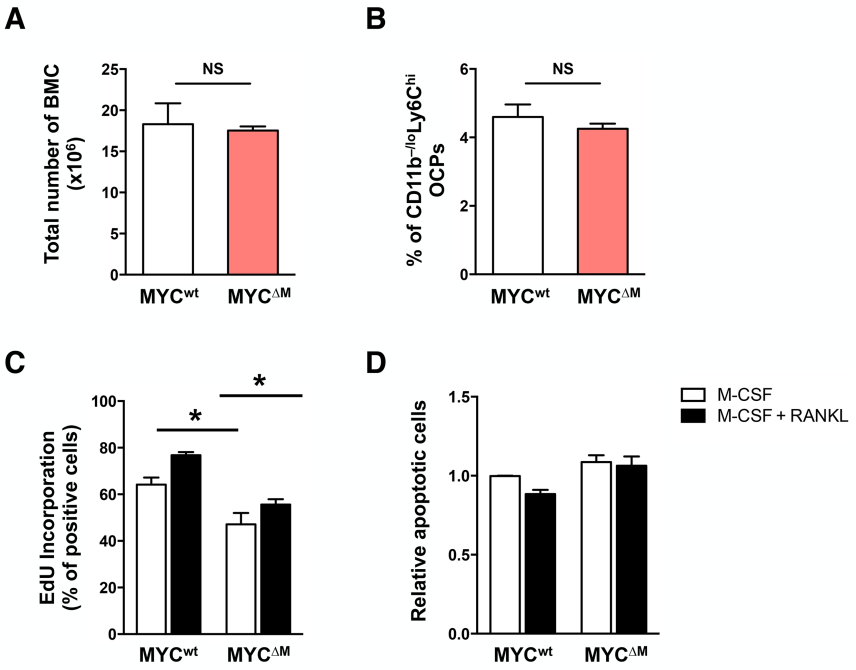

Supplemental Figure 4. Effect of MYC deficiency on the proliferation and survival of OCPs. (**A** and **B**) Mouse bone marrow cells (BMCs) were freshly flushed out from the femur of control (MYC^{wt}) and MYC-deficient ($MYC^{\Delta M}$) mice. (**A**) The total number of BMCs was counted ($n \geq 5$). (**B**) The frequency of $CD11b^{-/lo}Ly6C^{hi}$ cell population, previously described as osteoclast progenitors (1), in BMCs was measured by flow cytometry. (MYC^{wt}, $n=5$; $MYC^{\Delta M}$, $n=14$). (**C**) Cell proliferation rate (EdU incorporation assay, $n=5$) and (**D**) apoptosis (Annexin V^+ $7AAD^+$ staining, $n=2$) of control and MYC-deficient OCPs were analyzed after RANKL (50 ng/ml) stimulation for 24 hrs. All data are shown as mean ± SEM. $^*P < 0.05$ by Two-tailed, unpaired *t*-test in a,b, Two-way ANOVA with a *post hoc* Tukey test in c,d; NS, not significant.

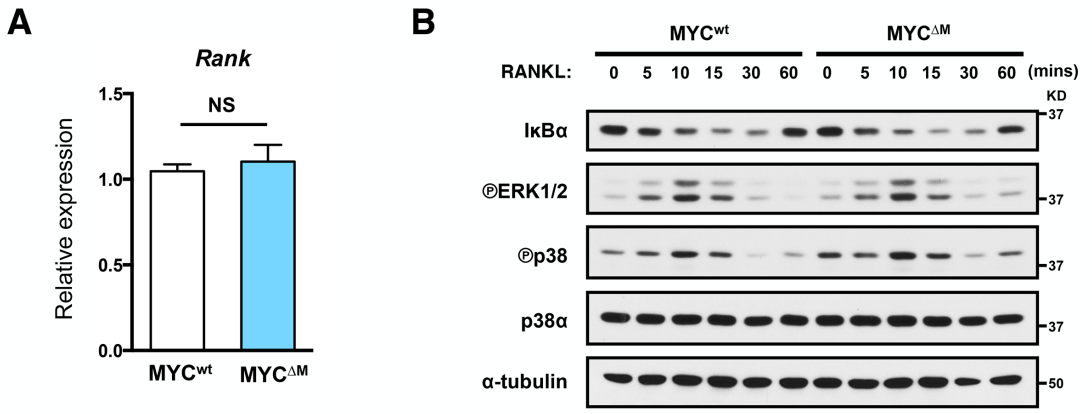

Supplemental Figure 5. Effect of MYC deficiency on the proximal RANKL signaling.

(**A**) The mRNA expression of *Rank* (relative to the *Hprt* housekeeping gene) in control (MYC^{wt}) and MYC-deficient ($MYC^{\Delta M}$) OCPs (*n*=3). Data are shown as mean ± SEM. NS, not significant by Two-tailed, unpaired *t*-test. (**B**) Control and MYC-deficient OCPs were stimulated with RANKL (100 ng/ml) for the indicated times. Whole-cell lysates were subjected to immunoblotting with the indicated antibodies. Data are representative of 3 experiments

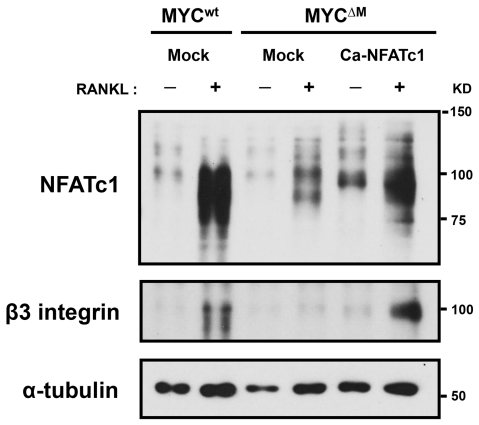

Supplemental Figure 6. Expression of NFATc1 and β3 integrin in mock-infected or constitutively active form of NFATc1 (ca-NFATc1)-transduced MYC-deficient OCPs.

Mock-infected or ca-NFATc1-transduced cells were cultured with or without RANKL (50 ng/ml) for 3 days, and whole-cell lysates were subjected to immunoblotting with the indicated antibodies. Overexpression of Ca-NFATc1 successfully induces β3 integrin, a target of NFATc1 (2). α-tubulin served as a loading control. Representative results from 3 experiments are shown.

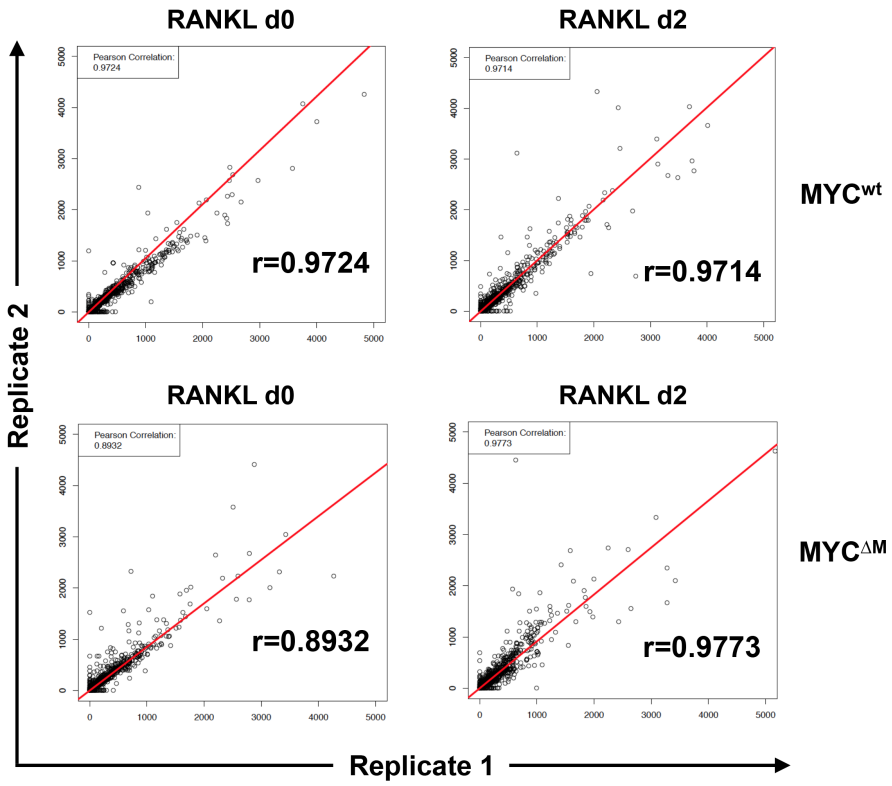

Supplemental Figure 7. Pearson correlation analysis of RNAseq data from two biological replicates.

Control (MYC^{wt}) and MYC-deficient ($MYC^{\Delta M}$) OCPs were stimulated with RANKL (50 ng/ml) for 2 days. The scatter plot diagrams show Pearson correlation analysis of gene expression profiles of two biological replicates. The red lines in the scatter plots show the linear model trend line of the data. The first replicate is plotted on the Y-axis and the second replicate on the X-axis. The respective correlation coefficient values are reported in each plot. Pearson correlation coefficients were >0.89, showing similarity of gene expression in biological replicates.

Top Canonical Pathway	
Name	P-value
Oxidative Phosphorylation	1.24E-29
Mitochondrial Dysfuction	1.58E-27
TCA Cycle II	2.48E-14
Acetyl-CoA Biosynthesis	7.22E-07
tRNA Charging	2.46E-06

Supplemental Figure 8. Ingenuity pathway analysis (IPA) analysis of MYC-dependent genes on day 2 after RANKL stimulation whose expression was suppressed in MYC-deficient OCPs.

Control (MYC^{wt}) and MYC-deficient ($MYC^{\Delta M}$) OCPs were stimulated with RANKL (50 ng/ml) for 2 days. To identify MYC-dependent genes for pathway analysis, we selected genes that were suppressed by MYC-deficiency (> 1.5 fold) at 2 days after RANKL stimulation (Figure 3A). These gene sets were analyzed by IPA in Supplemental Figure 7 and by gene set enrichment analysis (GSEA) in Table 1.

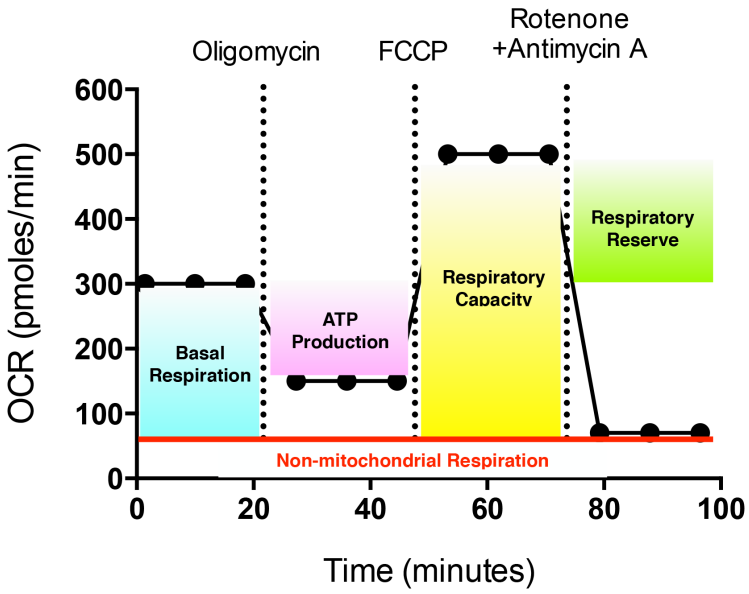

Supplemental Figure 9. A method of obtaining individual components of oxygen consumption rate (OCR) in Figures 3 and 5.

Upon the completion of real-time OCR measurement after sequential injection of indicated inhibitors modulating mitochondrial function, Basal Respiration, ATP Production, Respiratory Capacity, and Respiratory Reserve were calculated by quantifying area under the curve of the above graph following the manufacturer's protocol.

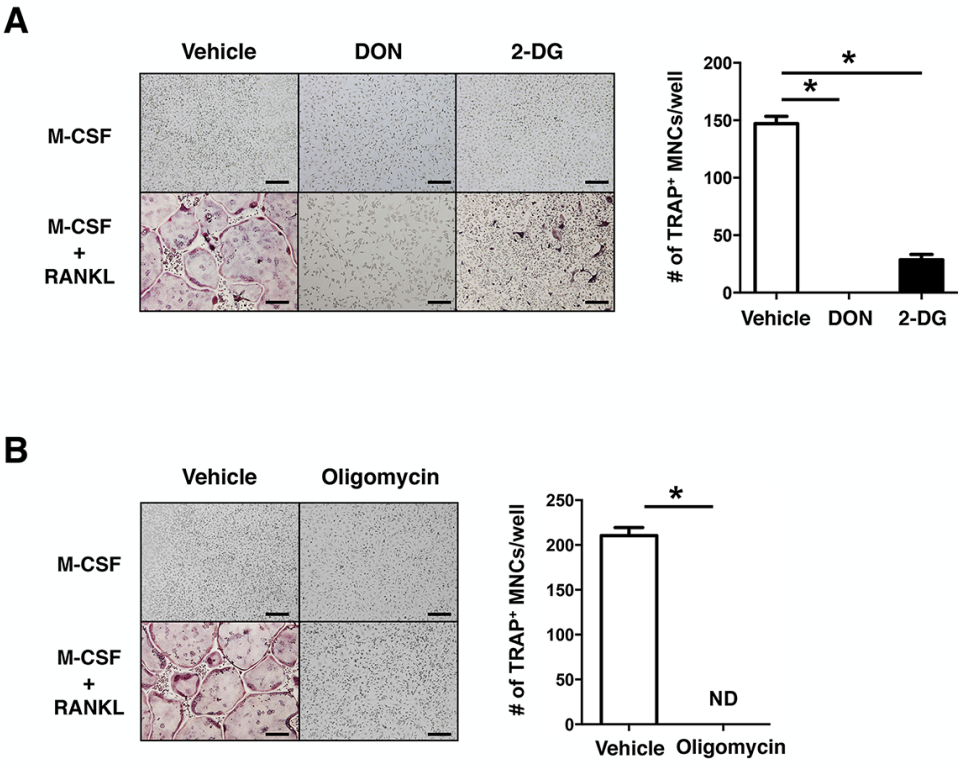

Supplemental Figure 10. Metabolic reprograming is required during osteoclast differentiation.

Mouse OCPs were treated with the (**A**) antagonists of glutaminolysis (6-Diazo-5-oxo-L-norleucine, DON, 0.1 mM), glycolysis (2-Deoxy-D-glucose, 2-DG, 0.1 mM), or (**B**) mitochondrial ATP synthesis (oligomycin, 1 nM) for an hour and then were stimulated with RANKL (50 ng/ml). Left panel shows a representative image of TRAP-stained cells. Scale bars, 200 µm. Right panel shows the number of TRAP-positive, multinucleated cells (MNCs) counted from at least 3 experiments. All data are shown as mean ± SEM. *$P < 0.05$ by One-way ANOVA with a *post hoc* Tukey test in **A**, Two-tailed, unpaired *t*-test in **B**. ND, not detected.

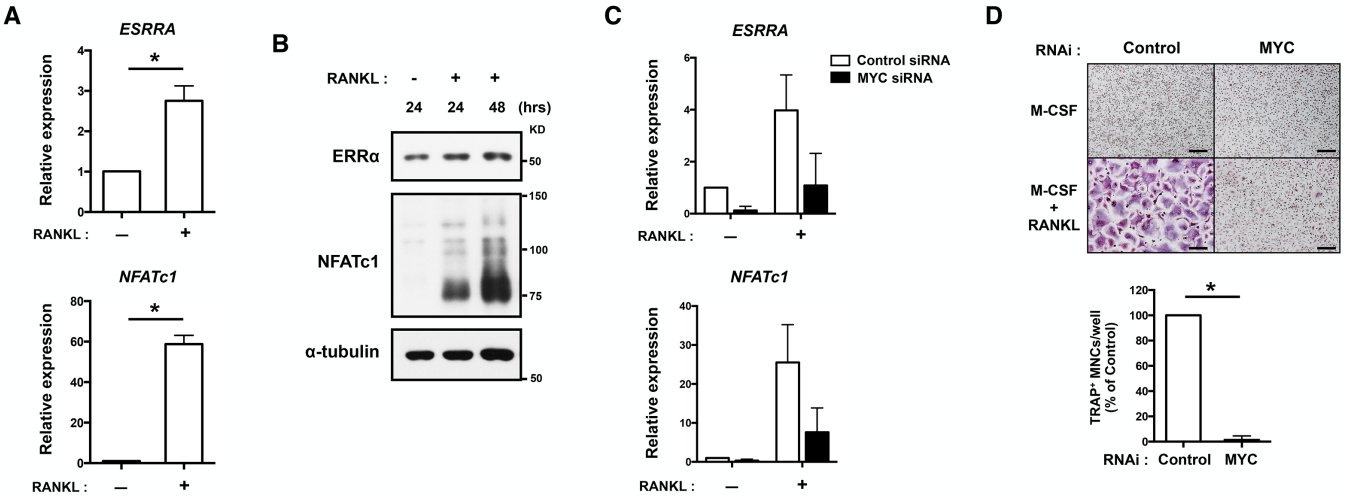

Supplemental Figure 11. MYC regulates ERRα expression in human osteoclastogenesis.

(**A** and **B**) Human OCPs were stimulated with RANKL (40 ng/ml) for the indicated time points. (**A**) The mRNA expression of *ESRRA and NFATc1* (relative to the *TBP* housekeeping gene) after RANKL stimulation for 48 hrs. Data are shown as mean ± SEM from four independent donors. **P* < 0.05 by Two-tailed, unpaired *t*-test. (**B**) The protein expression of ERRα and NFATc1 was determined by immunoblot using whole-cell lysates after RANKL stimulation for the indicated times. α-tubulin served as a loading control. Representative results from four independent donors are shown. (**C** and **D**) Human monocytes were nucleofected with control or MYC-specific small interfering RNAs (siRNAs) and then stimulated with RANKL (40 ng/ml). (**C**) The mRNA expression of *ESRRA and NFATc1* (relative to the *TBP* housekeeping gene) at two days following RANKL stimulation. Data are shown as mean ± SEM from three independent donors. (**D**) Osteoclastogenesis assay. Upper panel shows the representative images of TRAP-stained cells. Scale bars, 200 μm. Bottom panel shows the number of TRAP-positive, multinucleated cells (MNCs) counted in triplicate from five independent donors. Data are shown as mean ± SEM. **P* < 0.05 by Two-tailed, unpaired *t*-test.

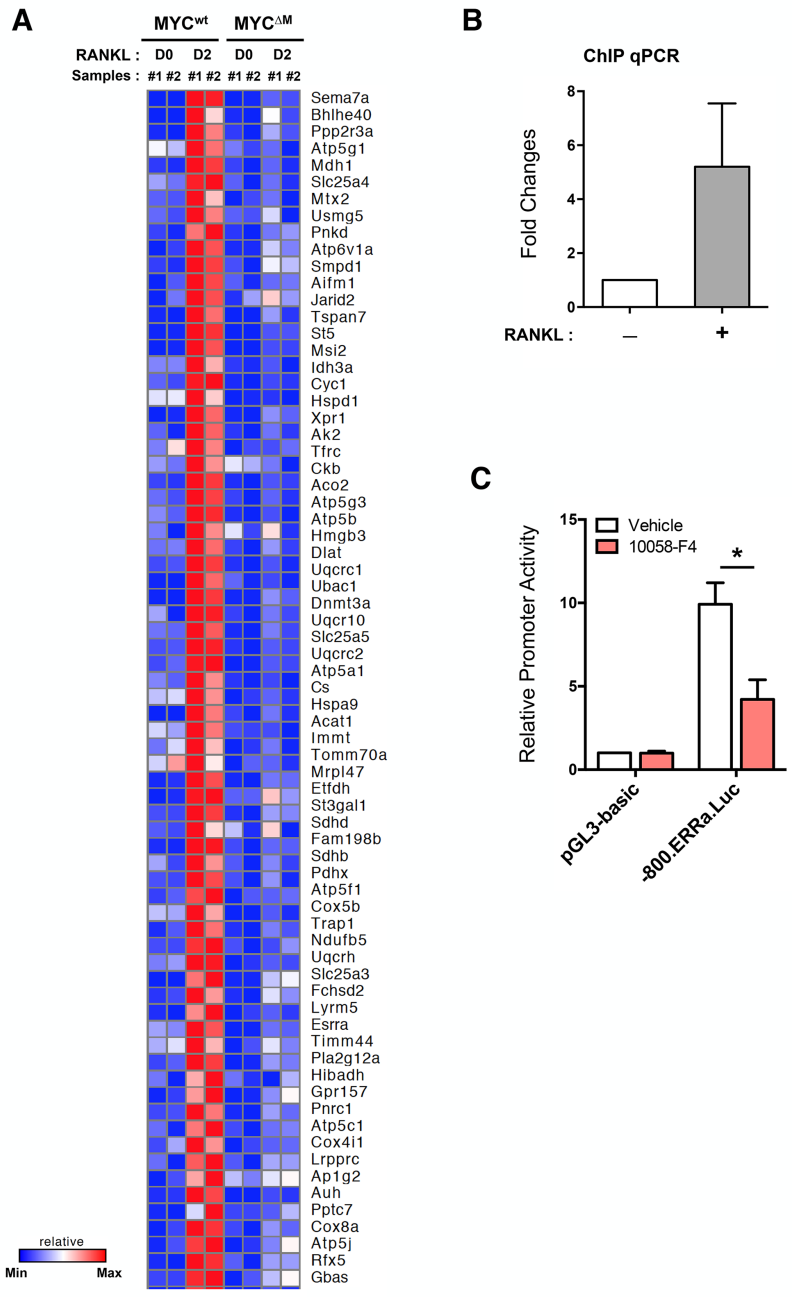

Supplemental Figure 12. MYC directly regulates ERRα in osteoclastogenesis.

(**A**) Heat map of RNA-seq FPKM values for ERRα target genes in control (MYC^{wt}) and MYC-deficient ($MYC^{\Delta M}$) OCPs following RANKL stimulation for 2 days. RNA-seq data from two biological replicates were used. To generate heat maps, we used GENE-E (Broad Institute) set to global comparison. (**B**) Chromatin immunoprecipitation (ChIP) realtime PCR analysis of the ERRα promoter for MYC. Human OCPs were stimulated with RANKL (40 ng/ml) for 24 h. Fold

changes of % input relative to the M-CSF condition are shown from 3 independent experiments with different donors. Data are shown as mean ± SEM. (**C**) RAW264.7 cells were transfected with an ERRα-luciferase reporter construct (-800.ERRα.Luc) or control (pGL3-basic) and stimulated with M-CSF (10 ng/ml) and RANKL (100 ng/ml) with the treatment of DMSO (vehicle control) or an MYC inhibitor 10058-F4 (50 μM). Fold inductions of the promoter activity relative to the pGL3-vehicle condition are shown (n=3). Data are shown as mean ± SEM. *$P < 0.05$ by Two-way ANOVA with a *post hoc* Tukey test.

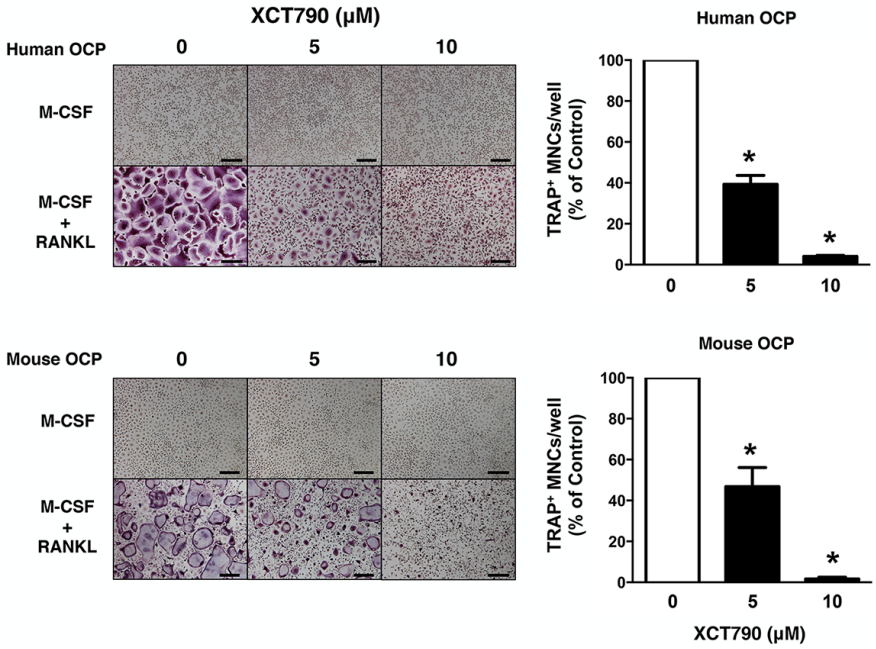

Supplemental Figure 13. ERRα inhibition suppresses osteoclast differentiation.

Human or mouse OCPs were co-cultured with RANKL (50 ng/ml) and ERRα antagonist (XCT790) at the indicated doses. Left panel shows the representative images of TRAP-stained cells. Scale bars, 200 μm. Right panel shows the number of TRAP-positive, multinucleated cells (MNCs) counted in triplicate from at least 3 experiments. All data are shown as mean ± SEM. *$P < 0.05$ by One-way ANOVA with a *post hoc* Tukey test.

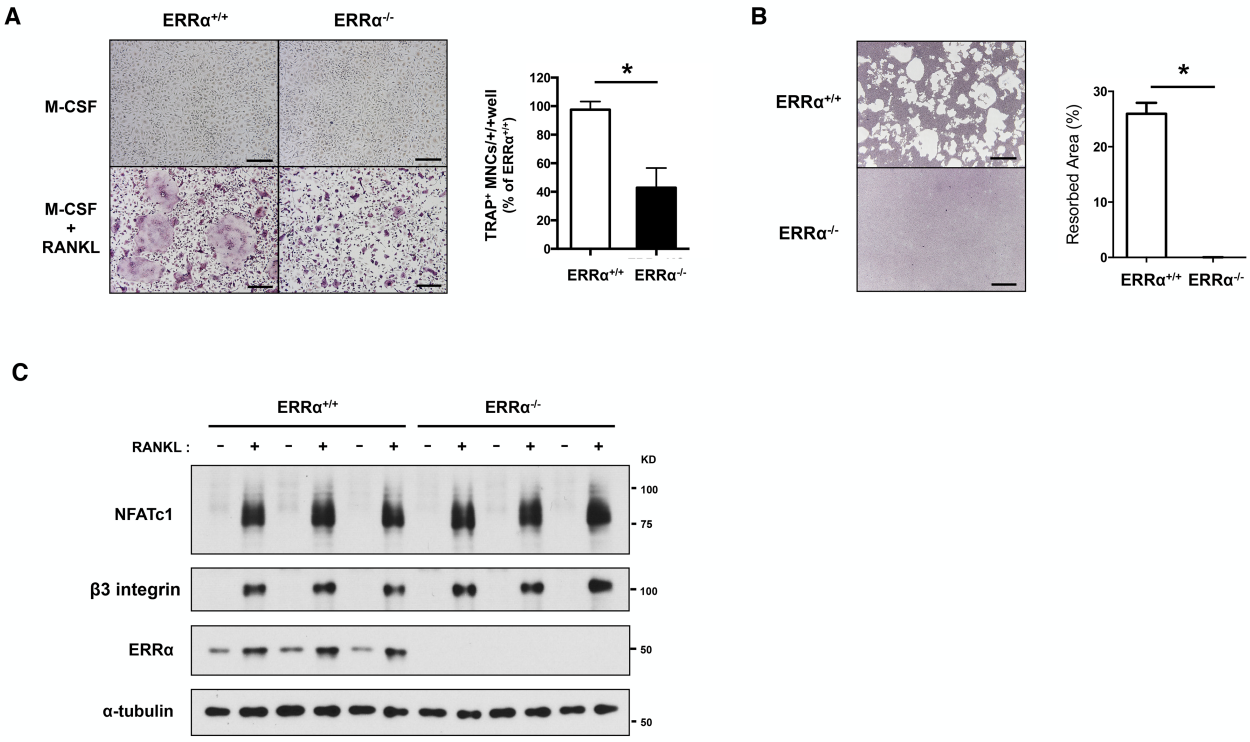

Supplemental Figure 14. ERRα deficiency exhibits defects of osteoclast differentiation and function.

(**A**) Osteoclast differentiation in control (ERRα$^{+/+}$) and ERRα-deficient (ERRα$^{-/-}$) OCPs stimulated with RANKL (50 ng/ml). Right panel shows the number of TRAP-positive, multinucleated cells (MNCs) counted in triplicate from 2 experiments (3 mice/group/experiment; *n*=6). Left panel shows the representative images. Scale bars, 200 μm. (**B**) Bone resorption activity of ERRα$^{+/+}$ and ERRα$^{-/-}$ OCPs stimulated with RANKL. Right panel shows the percentage of resorbed pit area per total area (*n*=5). Left panel shows the representative images. Scale bars, 200 μm. (**C**) Immunoblot of whole-cell lysates using NFATc1, β3 integrin, and α-tubulin antibodies. α-tubulin served as a loading control. All data are shown as mean ± SEM. **P* < 0.05 by Two-tailed, unpaired *t*-test.

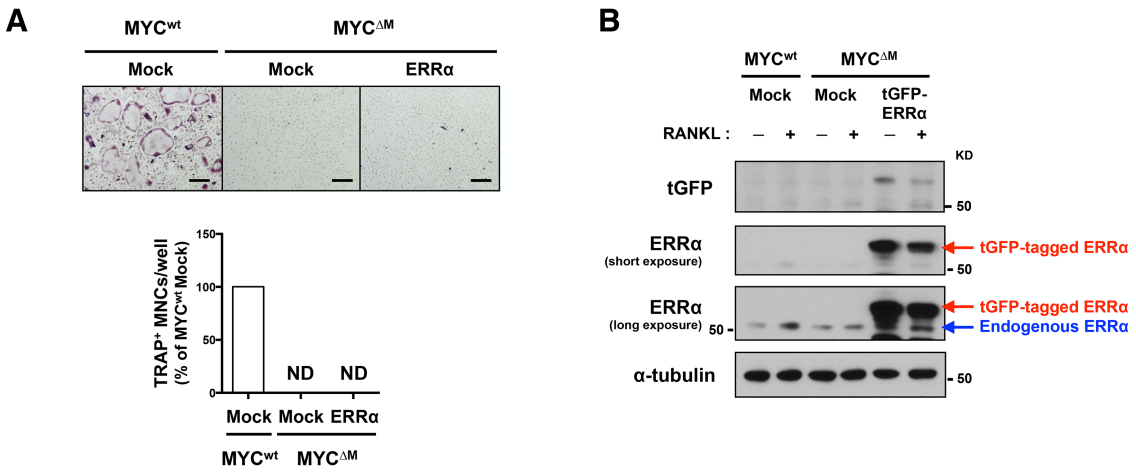

Supplemental Figure 15. Retroviral transduction of ERRα in MYC-deficient OCPs does not rescue osteoclastogenesis.

(**A**) Osteoclast differentiation in mock-infected or tGFP-tagged ERRα-transduced MYC-deficient ($MYC^{\Delta M}$) OCPs. Left panel shows the representative image of TRAP-stained cells. Scale bars, 200 μm. Right panel shows the number of TRAP-positive MNCs counted in triplicate from at least 3 experiments. Data are shown as mean ± SEM. ND, not detected. (**B**) Mock-infected or tGFP-tagged ERRα-transduced cells were cultured with or without RANKL (50 ng/ml) for 3 days, and whole-cell lysates were subjected to immunoblotting with the indicated antibodies. α-tubulin served as a loading control. Representative results from 3 experiments are shown.

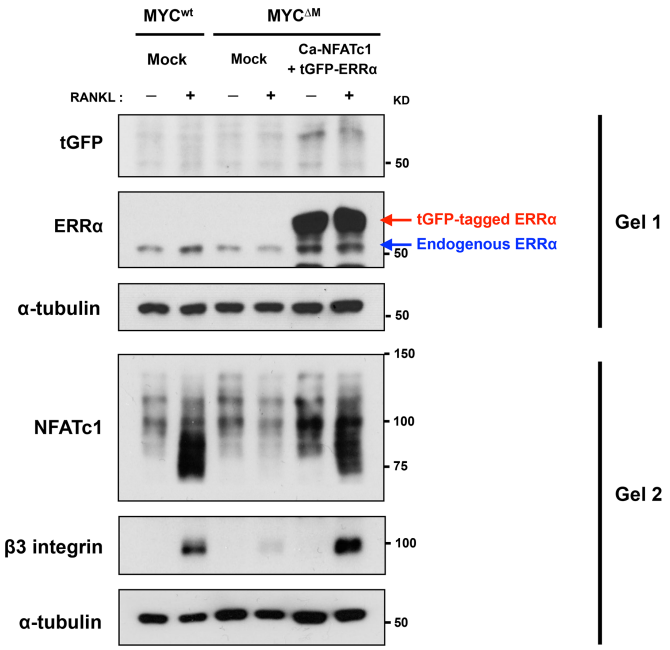

Supplemental Figure 16. Expression of NFATc1, β3 integrin, and ERRα in mock-infected or constitutively active form of NFATc1 (ca-NFATc1) and ERRα-transduced MYC-deficient OCPs.

Mock-infected or Ca-NFATc1 and ERRα-transduced cells were cultured with or without RANKL (50 ng/ml) for 3 days, and whole-cell lysates were subjected to immunoblotting with the indicated antibodies. α-tubulin served as a loading control. Representative results from 3 experiments are shown.

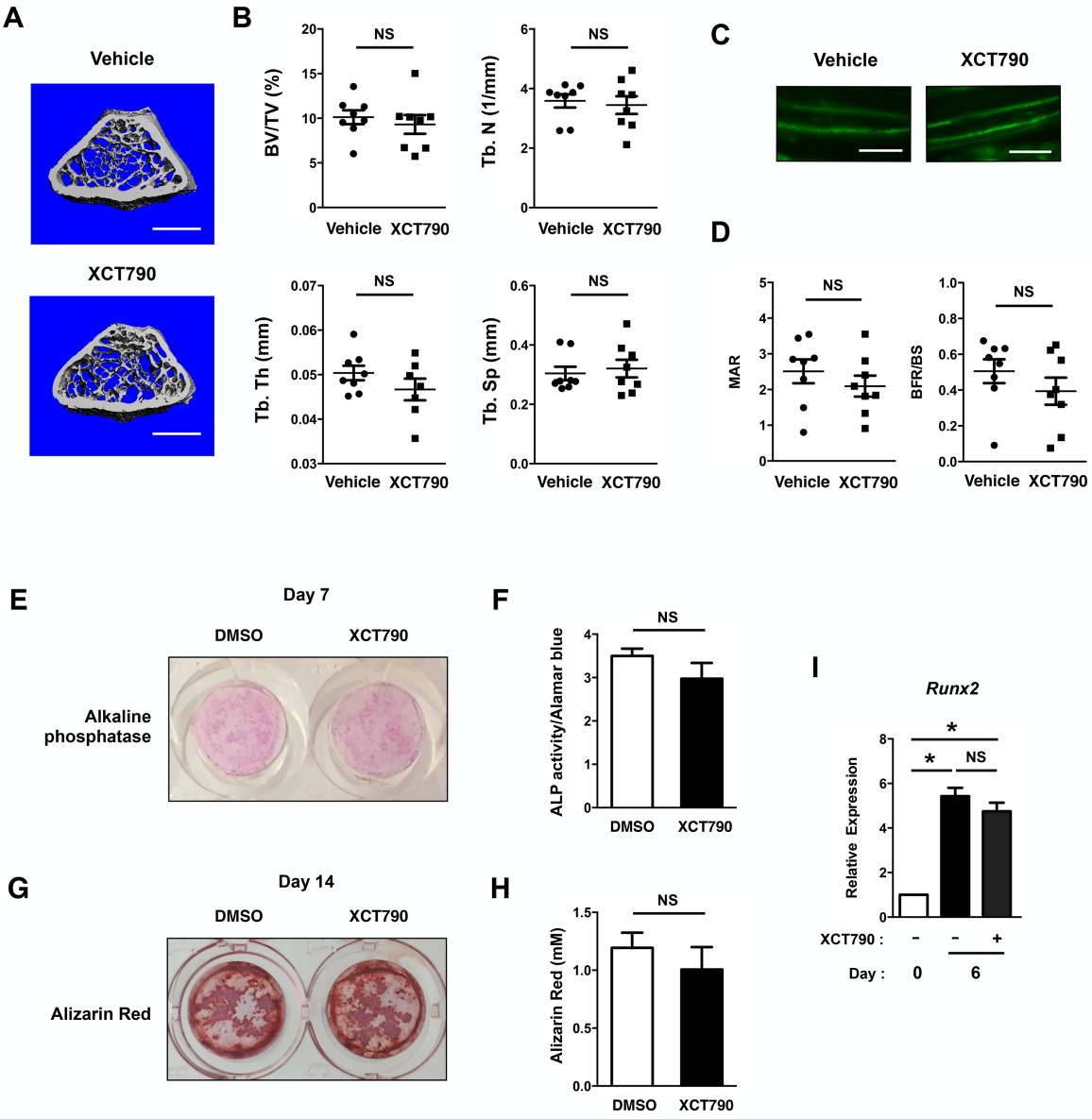

Supplemental Figure 17. The effect of ERRα inhibition in osteoblast differentiation.

(**A** and **B**) μCT analysis of the femurs of sham-operated, vehicle-treated (vehicle) and XCT790-treated (XCT790) CD-1 mice (*n*=8). Experimental design is same as Figure 7. Administration of vehicle or XCT790 started at 3 weeks following the surgery and continued for 5 weeks. (**A**) Representative images showing trabecular architecture by μCT reconstruction in the distal femurs. Scale bars, 1 mm. (**B**) μCT measurements for the indicated parameters in the distal femurs. Bone volume (BV/TV), trabecular number (Tb.N.), trabecular thickness (Tb.Th.), and

trabecular space (Tb.Sp.) were determined by μCT analysis. Data are shown as mean ± SEM. NS, not significant by Two-tailed, unpaired *t*-test. (**C** and **D**) Bone formation parameters including mineral apposition rate (MAR) and bone formation rate (BFR) were measured in sham-operated vehicle treated (Vehicle) and XCT790 treated mice (*n*=8). (**C**) Representative images showing calcein double labeling in trabecular bone. Scale bars 25 μm. (**D**) Bone formation parameters in distal femurs. BS, bone surface. Data are shown as mean ± SEM. NS, not significant by Two-tailed, unpaired *t*-test. (**E** to **I**) Primary calvarial osteoblasts were cultured in differentiation-inducing medium containing ascorbic acid and β-glycerophosphate, and osteoblast differentiation analyses were performed at the indicated times (*n*=3). Cells were treated with either DMSO or XCT790 (5 μM) from the beginning of the culture. (**E** and **F**) Alkaline phosphatase (ALP) activity was measured by colorimetric analysis at day 7. (**E**) Representative result of ALP staining. (**F**) Relative ALP activity was normalized by Alamar Blue fluorescence. Data are shown as mean ± SEM. NS, not significant by Two-tailed, unpaired *t*-test**.** (**G** and **H**) Mineralization activity was analyzed by alizarin red staining at day 14. (**G**) Representative result of alizarin red staining. (**H**) Alizarin red levels were measured by colorimetric quantification. Data are shown as mean ± SEM. NS, not significant by Two-tailed, unpaired *t*-test**. (I**) The mRNA expression of *Runx2* gene (relative to the *Gapdh* housekeeping gene) at the indicated times. Data are shown as mean ± SEM. **P* < 0.05; NS, not significant by Two-way ANOVA with a *post hoc* Tukey test.

Supplementary Methods

Human osteoclast differentiation

Peripheral blood mononuclear cells were obtained from blood leukocyte preparations purchased from the New York Blood Center by density gradient centrifugation with Ficoll (Invitrogen, Carlsbad, CA) using a protocol approved by the Hospital for Special Surgery Institutional Review Board. Monocytes were obtained from peripheral blood using anti-CD14 magnetic beads, as recommended by the manufacturer (Miltenyi Biotec Auburn, CA), and the purity of monocytes was >97%, as verified by flow cytometric analysis. Isolated cells were added to 96 well plates in triplicate at a seeding density of $1x10^5$ cells per well, and monocyte-derived osteoclast precursors (OCPs) that express RANK were obtained by culturing for one day with 20 ng/ml of M-CSF (Peprotech) in α-MEM medium (Invitrogen) supplemented with 10% fetal bovine serum (FBS, Hyclone). OCPs were incubated with 20 ng/ml of M-CSF and 40 ng/ml of human soluble RANKL (Peprotech) for four additional days in α-MEM supplemented with 10 % FBS. Cytokines were replenished every 3 days. Cells were fixed and stained for TRAP using the Acid Phosphatase Leukocyte diagnostic kit (Sigma) as recommended by the manufacturer. Multinucleated (more than 3 nuclei), TRAP-positive osteoclasts were counted in triplicate wells. Imaging was performed with a 10X objective.

Flow cytometry

The $CD11b^{-/lo}Ly6C^{hi}$ osteoclast precursor population was determined as previously described (1). Briefly, freshly isolated BM cells were blocked with anti-mouse CD16/CD32 (553141, BD Biosciences), followed by incubation with a mix of Ter119-PE, CD3e-PE (130102336, 130102600 respectively; Miltenyi Biotec), B220-PE, CD11b-APC, and Ly6C-PerCP (553089, 553312, 560525 respectively, BD Biosciences). After exclusion of $CD3^+/B220^+/Ter119\text{-}PE^+$ cells, cells were gated based on CD11b and Ly6C staining intensity. The rate of cell proliferation was determined using Click-iT Plus EdU Alexa Fluor 647 Kit (Molecular Probes) following the manufacturer's protocol, and apoptotic cells were detected after annexin V and 7AAD labeling following the manufacturer's protocol (BD Biosciences). To label mitochondria, cells were incubated with 20 nM of MitoTracker Deep Red FM (Molecular Probes), which passively diffuses across the plasma membrane and accumulate in active mitochondria, for 30 min at 37°C. After washing twice with cold PBS containing 0.5% BSA, cells were analyzed. Flow cytometry was performed on a FACS Scan or Calibur (BD Biosciences) and analyzed with FlowJo software (Tree Star Inc., Ashland, OR).

Retroviral plasmid constructs

The retroviral vector expressing constitutively active version of NFATc1 (pMSCV-caNFATc1) was kindly provided by Dr. Yongwon Choi (University of Pennsylvania, Philadelphia, PA) (3). ERRα gene was amplified using PCR primers from the mouse estrogen related receptor, alpha (*Esrra)* cDNA ORF clone (MR225753, OriGene Technologies, MD) with the following primers: Forward: 5'- GGGATCCATGTCCAGCCAGGTGGTGGGCATC-3' and Reverse: 5'- GGGAATTCCGTTTAAACCTTATCGTCGT-3'. Then, ERRα genes were ligated into the retroviral vector, pMX-puro to generate pMX-puro-ERRα. The retroviral vector pMX-MYC (Plasmid #13375) and its control vector (Plasmid #18656) were purchased from Addgene.

RNA interference

0.2 nmol of short interfering RNAs (siRNAs), specifically targeting human MYC (Invitrogen; 1299001; HSS106837), or non-targeting control siRNAs (Ambion; AM4636) were transfected into primary human $CD14^+$ monocytes with the Amaxa Nucleofector device set to program Y-001 using the Human Monocyte Nucleofector kit (Amaxa), as previously described (4).

Chromatin Immunoprecipitation (ChIP)

ChIP was performed as previously described (5). Briefly, 3 x 10^7 human primary OCPs were fixed by adding formaldehyde directly to the medium to a final concentration of 1 % for 5 min. Cells were harvested, washed, and lysed. Chromatin was sheared by sonication to a length of approximately 500 base pairs using a Bioruptor sonicator (Diagenode). Sheared chromatin was precleared and then immunoprecipitated with anti-c-myc antibody (Santa Cruz Biotechnology; sc764). Immune complexes were subsequently collected and washed, and DNA crosslinking was reversed by heating at 65^{o}C overnight. Following proteinase K digestion, DNA was recovered using the PCR purification kit (Qiagen) and real time PCR was performed to detect the occupancy of target proteins. Signals obtained from the ChIP are divided by signals obtained from an input sample. This input sample represents the amount of chromatin used in the ChIP. The primer sequences are listed in Supplemental Table 1.

Luciferase assay

The -800.ERRα.Luc reporters cloned into pGL3-Basic vector (Promega) were kindly provided by Dr. Janice Huss (City of Hope National Medical Center, Duarte, CA) (6) and transfected into Raw 264.7 cells using Amaxa Cell Line Nucleofector Kit V (Lonza). At 20 hr after transfection,

cell extracts were prepared by adding 100 μL of 1x Passive Reporter Lysis Buffer (Promega), and luciferase activity was analyzed with the Dual-Glo Luciferase Assay System (Promega), according to the manufacturer's protocol. Firefly luciferase was normalized to the activity of *Renilla* luciferase driven by the CMV promoter.

Mice

Esrra-deficient and control female mice, both eight weeks old, were kindly provided by Dr. Vincent Giguère (McGill University, Montréal, Canada).

Analysis of bone phenotype

To measure bone mineralization, mice were intraperitoneally injected with Calcein (green; Sigma) at 10 μg/g (body weight) twice at 7 days apart. Two days after the second injection, femurs were collected, fixed in 4% paraformaldehyde, and embedded in OCT compound (Thermo Fisher Scientific, Waltham, MA) as described previously (7), and then cut into 7-μm sections. Histomorphometry analysis using the OsteoMetrics software (OsteoMeasure) was performed on trabecular bone within the femoral metaphysis. Mineral apposition rate (MAR) was determined by measuring the distance between two fluorochrome-labeled mineralization fronts. The mineralizing surface was determined by measuring the double-labeled surface and one-half of single labeled surface and expressing this value as the percentage of total bone surface. The bone formation rate was expressed as MAR x mineralizing surface/total bone surface, using a surface referent.

Osteoblast differentiation analysis

For osteoblast differentiation assay, ALP activity, extracellular matrix mineralization, and osteoblast marker gene expression were analyzed. Primary osteoblast precursors were isolated from calvaria of 3 day old CD-1 mice by using the digestion solution containing type II collagenase and dispase I (Invitrogen). Cells were cultured with α-MEM containing 10% FBS, 50 μg/ml of ascorbic acid, and 8 mM beta-glycerophosphate. For alkaline phosphatase (ALP) staining, osteoblasts were incubated with 10-fold diluted Alamar Blue solution (Invitrogen), washed, and incubated with a phosphatase substrate solution (Sigma-Aldrich), and ALP activity was measured by colorimetric analysis at 405 nm. Results were normalized to Alamar Blue fluorescence and shown as relative ALP activity. For osteoblast marker gene expression, total mRNA was purified from osteoblast cultures at day 0, 6, and 12. Real time PCR was performed in triplicate using the iCycler iQ thermal cycler and detection system (Applied Biosystems,

Carlsbad, CA) following the manufacturer's protocols. Expression of the tested gene was normalized relative to levels of *Gapdh*. The primer sequences are listed in Supplemental Table 1. To quantify mineralization activity, cells were fixed at day 14 with cold 70% ethanol and stained with alizarin red S (10 mg/ml), and alizarin red levels were measured by colorimetric quantification at 405 nm.

Statistical analysis

All statistical analyses were performed with Graphpad Prism 5.0 software using the two-tailed, unpaired *t*-test (two conditions), One-way or Two-way ANOVA for multiple comparisons (more than two conditions) with a *post hoc* Tukey test. $P < 0.05$ (*) was taken as statistically significant.

Supplemental Table 1. A list of primers used in this study:

Gene Symbol	Sequence
Myc	CGACTACGACTCCGTACAGC GTAGCGACCGCAACATAGGA
Nfatc1	CCCGTCACATTCTGGTCCAT CAAGTAACCGTGTAGCTCCACAA
Itgb3	CCGGGGGACTTAATGAGACCACTT ACGCCCCAAATCCCACCCATACA
CtsK	AAGATATTGGTGGCTTTGG ATCGCTGCGTCCCTCT
Dcstamp	CTCGCCGGGCTTCTGCTCAT CCGCTGTTGGTGCCTCTCCT
Esrra	CAGGATCTGCCCAGCATAGG GCTTCTGACAATCCCCCACA
Idh3a	TGGCCCAGAAATTTCAGCCT ATTGCTGTGACATTGCGCTC
Sdhb	GCAGTTTCAGGCCTGTCGAG TCGTACGTCTGCATTCGAGG
Cyc1	GGAGGCAAGCATAAGACTGG TCCATCAGGGTATCCTCTCC
Cox5b	GCAGTTTCAGGCCTGTCGAG TCGTACGTCTGCATTCGAGG
Uqcrc2	GCAGTTTCAGGCCTGTCGAG TCGTACGTCTGCATTCGAGG
Runx2	TACAAACCATACCCAGTCCCTGTTT AGTGCTCTAACCACAGTCCATGCA
Gapdh	ATCAAGAAGGTGGTGAAGCA AGACAACCTGGTCCTCAGTGT
Hprt	TCCTCAGACCGCTTTTTGCC CTAATCACGACGCTGGGACT
NFATc1	CTTCTTCCAGTATTCCACCTAT TTGCCCTAATTACCTGTTGAAG
ESRRA	CCCATGCCTGCCCGAC GTCTCCGAGGAACCCTTTGG

TBP	CACCACAGCTCTTCCACTA GGGGAGGGATACAGTGGAGT

ERRα promoter	ACCTTGAGCTTTCTCCGTCC CGAACCGTAGACCCAGTAGC

Supplemental References

1. Charles JF, Hsu LY, Niemi EC, Weiss A, Aliprantis AO, and Nakamura MC. Inflammatory arthritis increases mouse osteoclast precursors with myeloid suppressor function. *J Clin Invest.* 2012;122(12):4592-605.
2. Aliprantis AO, Ueki Y, Sulyanto R, Park A, Sigrist KS, Sharma SM, Ostrowski MC, Olsen BR, and Glimcher LH. NFATc1 in mice represses osteoprotegerin during osteoclastogenesis and dissociates systemic osteopenia from inflammation in cherubism. *J Clin Invest.* 2008;118(11):3775-89.
3. Kim K, Kim JH, Lee J, Jin HM, Lee SH, Fisher DE, Kook H, Kim KK, Choi Y, and Kim N. Nuclear factor of activated T cells c1 induces osteoclast-associated receptor gene expression during tumor necrosis factor-related activation-induced cytokine-mediated osteoclastogenesis. *J Biol Chem.* 2005;280(42):35209-16.
4. Park-Min KH, Serbina NV, Yang W, Ma X, Krystal G, Neel BG, Nutt SL, Hu X, and Ivashkiv LB. FcgammaRIII-dependent inhibition of interferon-gamma responses mediates suppressive effects of intravenous immune globulin. *Immunity.* 2007;26(1):67-78.
5. Nicodeme E, Jeffrey KL, Schaefer U, Beinke S, Dewell S, Chung CW, Chandwani R, Marazzi I, Wilson P, Coste H, et al. Suppression of inflammation by a synthetic histone mimic. *Nature.* 2010;468(7327):1119-23.
6. LaBarge S, McDonald M, Smith-Powell L, Auwerx J, and Huss JM. Estrogen-related receptor-alpha (ERRalpha) deficiency in skeletal muscle impairs regeneration in response to injury. *FASEB J.* 2014;28(3):1082-97.
7. Yeon Won H, Hwan Mun S, Shin B, and Lee SK. Contradictory Role of CD97 in Basal and Tumor Necrosis Factor-Induced Osteoclastogenesis In Vivo. *Arthritis Rheumatol.* 2016;68(5):1301-13.